Astrocyte Activation Imaging with ^{11}C-Acetate and Amyloid PET in Mild Cognitive Impairment due to Alzheimer Pathology

Michael Tran Duong[1,2,3], **Yin Jie Chen**[1], **Robert K. Doot**[1], **Anthony J. Young**[1], **Hsiaoju Lee**[1], **Jenny Cai**[1], **Arun Pilania**[2], **David A. Wolk**[2,3], **Ilya M. Nasrallah**[1,3]

[1]Division of Nuclear Medicine, Department of Radiology, Perelman School of Medicine, University of Pennsylvania

[2]Penn Memory Center, Department of Neurology, Perelman School of Medicine, University of Pennsylvania

[3]Department of Bioengineering, School of Engineering and Applied Sciences, University of Pennsylvania

Abstract

Background.—Neuroinflammation is a well-known feature of early Alzheimer disease (AD) yet astrocyte activation has not been extensively evaluated with *in vivo* imaging in Mild Cognitive Impairment (MCI) due to amyloid plaque pathology. Unlike neurons, astrocytes metabolize acetate, which has potential as a glial biomarker in neurodegeneration in response to AD pathologic features. Since the medial temporal lobe (MTL) is a hotspot for AD neurodegeneration and inflammation, we assessed astrocyte activity in the MTL and compared to amyloid and cognition.

Methods.—We evaluate spatial patterns of *in vivo* astrocyte activation and their relationships to amyloid deposition and cognition in a cross-sectional pilot study of 6 participants with MCI and 5 cognitively normal (CN) participants. We measure ^{11}C-acetate and ^{18}F-florbetaben amyloid standardized uptake values ratios (SUVRs) and kinetic flux compared to cerebellum on positron emission tomography (PET), with magnetic resonance imaging and neurocognitive testing.

Results.—Medial temporal lobe (MTL) ^{11}C-acetate SUVR was significantly elevated in MCI compared to CN participants ($P = 0.03$; Cohen $d = 1.76$). Moreover, MTL ^{11}C-acetate SUVR displayed significant associations with global and regional amyloid burden in MCI. Greater MTL ^{11}C-acetate retention was significantly related with worse neurocognitive measures including the Montreal Cognitive Assessment ($P = 0.001$), Word List Recall memory ($P = 0.03$), Boston Naming Test ($P = 0.04$) and Trails B test ($P = 0.04$).

Conclusions.—While further validation is required, this exploratory pilot study suggests a potential role for ^{11}C-acetate PET as a neuroinflammatory biomarker in MCI and early AD to provide clinical and translational insights into astrocyte activation as a pathological response to amyloid.

---

[*]Correspondence: 3400 Civic Center Blvd, Philadelphia, PA 19104, United States.

Keywords

Alzheimer Disease; Cognition; Amyloid; Neuroinflammation; Astrocyte; Acetate; PET

INTRODUCTION

Neuroinflammation is a major pathological feature of Alzheimer disease (AD). Alzheimer and Fischer's 1907 discoveries identified the association between activated astrocytes and amyloid plaques [1,2], which was subsequently confirmed [3-5]. In AD, astrocyte activation is observed particularly in the hippocampus within the medial temporal lobe (MTL) [6]. Neuroinflammation in mild cognitive impairment (MCI) and AD has been studied most often through microglial imaging using positron emission tomography (PET) [7]. However, methods to evaluate astrocyte activation with *in vivo* metabolite-based imaging have not been extensively studied in MCI and AD.

Here, we explore astrocyte activation in MCI due to AD pathology using ^{11}C-acetate PET. Acetate is a metabolic substrate for astrocytes but not neurons, particularly when used for fatty acid synthesis and glial proliferation [8,9]. Astrocyte activation is a dynamic process comprising different activity states [6]. *Ex vivo* and *in vitro* findings demonstrate that activated astrocytes linked to AD will display intracellular accumulation of fatty acids and lipids [1,10,11]. These observations in AD support *in vivo* imaging results from other brain diseases showing that astrocyte proliferation and anabolism are associated with higher ^{11}C-acetate retention [12,13]. Since ^{11}C-acetate PET has already been applied to evaluate activated astrocytes in patients with multiple sclerosis [14], alcoholism [15] and glioma [16], we sought to test ^{11}C-acetate PET as a marker of astrocyte neuroinflammation in patients with MCI and amyloid pathology.

Guided by literature and analysis of *ex vivo* astrocyte markers (Supplement), we predicted that *in vivo* ^{11}C-acetate retention is elevated in the MTL. Furthermore, we posited that ^{11}C-acetate retention correlated with amyloid PET burden and with worse performance on tests of MTL-associated memory and global cognition. We emphasize that this pilot study is exploratory; while this inquiry cannot definitively answer these hypotheses, it can provide insight into the potential applications of ^{11}C-acetate PET in MCI and AD.

MATERIALS AND METHODS

Study Design and Participants

This cross-sectional imaging study (NIH NCT02811744) was approved by the Institutional Review Board of our hospital and evaluated participants over the age of 60 years old from 2016 to 2018. Informed consent was obtained by a physician. Participants with normal cognition and MCI were assessed for competence and accompanied by a study partner. Participants with MCI had amnestic phenotype and amyloid-positive PET, thus characterized as having MCI due to AD pathology. Both amyloid-positive and amyloid-negative participants with normal cognition were recruited. Though this diverse "control group" reduces the power to identify group differences in MCI, this approach more

realistically captures the heterogeneity in amyloid levels found in cognitively normal older adults. Moreover, such a cognitively normal (CN) group with both amyloid-negative and amyloid-positive participants provides a dynamic range of subclinical cerebral amyloid levels to identify possible relationships between regional ^{11}C-acetate and amyloid PET measures.

Magnetic Resonance Imaging

Isotropic T1 magnetization-prepared rapid gradient echo (MPRAGE; 0.8mm^3) magnetic resonance imaging (MRI) on a 3 Tesla scanner (Magnetom Prisma or Trio model, Siemens, Erlangen, Germany) with a 64-channel head coil were obtained within 111 ± 182 days of ^{11}C-acetate PET scan. There was no significant difference of time between ^{11}C-acetate and MRI for cognitively normal and MCI groups. MRIs were used for defining regions of interest (ROIs) and adjusting for atrophy-related cerebrospinal fluid dilution.

[11]C-Acetate PET

PET was performed on an Ingenuity TF PET/computed tomography (CT) scanner (Phillips Healthcare, Amsterdam, Netherlands) with low dose CT for attenuation correction. Reconstruction used BLOB-OS-TF with trans-axial field of view of 256mm and 2mm isotropic voxels. ^{11}C-Acetate was produced at our GMP cyclotron facility per established protocol [17]. Each subject was injected with about 20mCi (range 19-24mCi) as a rapid bolus with simultaneous initiation of a 60 minute, 50 frame dynamic acquisition (24x5 seconds, 6x10 seconds, 3x20 seconds, 2x30 seconds, 5x60 seconds, 10x300 seconds). Venous blood samples were collected at 2, 5, 10, 20, 40, and 60 minutes post-injection of ^{11}C-acetate to quantify the amount of the metabolite $^{11}C\text{-}CO_2$ in blood over time. Whole blood samples were mixed into a basic solution of 1-part 0.9M $NaHCO_3$, 3-parts isopropanol, and 1-part 0.1N NaOH and an acidic solution containing 1-part 0.9M $NaHCO_3$, 3-parts isopropanol, and 1-part 6N HCl. The basic solution was sealed, while the acidic solution was placed in a positive pressure manifold and exposed to an air current to release metabolized $^{11}C\text{-}CO_2$. Samples were counted in Wizard^2 2480 gamma counter (PerkinElmer, Waltham, MA, United States) to calculate percentage un-metabolized parent for kinetic analyses of tracer uptake.

Regional time-activity curves (TACs) were quantified using 30 ROIs determined from fused T1-weighted MRI in the PMOD package v3.7 (PMOD Technologies, Zurich, Switzerland) and the Automated Anatomical Labeling merged atlas [18]. Examples of TACs from the venous blood sampling and individual brain ROIs are shown in Figures S1 and S2, respectively. Regional TACs were quantified without and with partial volume correction (PVC) using geometric transfer ratio method implementation in PMOD [19]. Results are presented with PVC as findings without PVC are similar. Since AD and amnestic MCI demonstrate relatively symmetric, bilateral pathology of amyloid deposition [20-22], atrophy [23] and glial-mediated neuroinflammation [7], left and right ROIs were combined via volume-weighted average in regional analyses. Our cohort displayed right and left symmetry for both amyloid and ^{11}C-acetate imaging. The Heschl gyrus ROI was excluded from study analyses due to small size ($<1cm^3$) relative to our PET scanner's spatial resolution of 5mm full width at half maximum [24].

For static analysis, uptake from 40-60 minutes post-injection dynamic frames were averaged to generate standardized uptake value (SUV) parametric images. This timeframe was selected to preferentially capture ^{11}C-acetate trapped in biosynthetic pathways in activated astrocytes, rather than what was catabolized to ^{11}C-CO_2 [9,14,16,25]. SUV was normalized to cerebellar gray matter (GM) as a physiological comparator region to calculate SUV ratio (SUVR) [14,16]. Until late stages of AD (well beyond early stages in our sample), cerebellar GM is mostly free of amyloid deposition [7,26-28] and glial activation [7,29-31]. Unlike cerebellar white matter, the GM contains more abundant astrocytes, the cell type of interest. Thus, cerebellar GM astrocytes in MCI are not exposed to local amyloid-related neuropathologic changes so this region can serve as a comparator for astrocyte metabolism in the absence of Alzheimer pathology [29-31].

For kinetic modeling, image-derived arterial input functions were calculated per previously published methods [32] and were scaled using individual venous blood data from 10-60 minutes post-injection. Kinetic parameters of regional brain ^{11}C-acetate uptake were modeled in PMOD. TACs were fitted using Patlak graphical methods [33,34]. The model inputs included individual blood input functions and the population average ^{11}C-acetate parent fractions (Figure S1B). Plasma ^{11}C-acetate concentrations were assumed to be equal to whole blood concentrations. Brain blood volume fractions were fixed at 5%. Patlak linear analyses were performed to derive kinetic flux (Ki). Due to anticipated errors in kinetic modeling for ^{11}C-acetate from lack of invasive cannulated arterial input function, inherent limitations of image-derived input functions [35] and potential variability in biodistribution of the ^{11}C-CO_2 metabolite, we evaluated a flux ratio (KiR) based on nuclear medicine literature [36-40] with cerebellar GM as comparator region, similar to astrocyte imaging studies with ^{11}C-deuterium-L-deprenyl [29-31]. Kinetic flux was compared to cerebellar GM to normalize for variability in ^{11}C-acetate delivery, washout and background due to metabolism to ^{11}C-CO_2 in a region of baseline astrocyte activity without the presence of amyloid. Time stability curves of regional distribution volumes (V_T) were created with the Logan method [41] with PMOD. Dynamic PET scans were visualized on MIM (MIM Software Inc, Cleveland, OH, United States).

[18]F-Florbetaben PET

Amyloid PET was performed as 20-minute scans after 8.1mCi ^{18}F-florbetaben intravenous injection as per standard clinical protocol within 176±108 days prior to ^{11}C-acetate PET scan. SUV analyses were performed similar to methods described above. The SUVR reference region was the cerebellum, as described in literature [26,27]. A trained neuroradiologist interpreted amyloid scans as amyloid-positive or amyloid-negative per established qualitative guidelines [27]. There was no significant difference in the time between ^{11}C-acetate and ^{18}F-florbetaben PET scans for cognitively normal and MCI groups. One cognitively normal participant had ^{18}F-florbetapir PET and was excluded from comparisons of regional amyloid ^{18}F-florbetaben vs. ^{11}C-acetate but was included for other analyses.

Cognitive Evaluation

Cognitive testing was performed the day of ^{11}C-acetate PET and included the Word List Recall memory (10 word test) [42], Montreal Cognitive Assessment (MoCA) [43], Boston Naming Test (BNT) [44], Trail Making B Test [45] and Rey Auditory-Verbal Learning Test [46] per NIH AD Research Center (ADRC) guidelines.

Statistical Analysis

Descriptive statistics show mean and standard deviation unless otherwise specified. Analysis was performed with 2-sample independent means *t*-tests with 2-tailed *P* values. Effect size was computed with the Cohen *d* statistic. Due to the exploratory nature of these pilot study investigations, *P* values were not corrected for multiple comparisons and a threshold of *P* < 0.05 was considered statistically significant. With the goal of 0.80 power and 0.05 type I error, we predicted the sample size would be sufficient to detect mean SUVR difference of 0.1. Regressions for cognition and ^{11}C-acetate measures were evaluated with Spearman correlations. To evaluate amyloid and ^{11}C-acetate relationships across the 30 brain ROIs sampled within subjects, linear mixed-effects regression model analyses were performed using the nlme package in R v4.0.2 [47]. Fixed effects included regional ^{11}C-acetate measures and amyloid SUVR for each ROI in each participant. The participants served as random effects to account for the regional variation between individuals. Differences in correlations were determined by 2-tailed Fisher *R*-to-*Z* transformation. Differences in regressions were compared by 2-sample *t*-tests between slopes. Given the sample size, leave-one-participant-out analysis was performed to assess if individual participants were disproportionately influencing correlations; this did not change the results.

RESULTS

There were 6 participants with MCI (mean age 72±6 years) compared to 5 CN participants (74±10 years, 3 amyloid-positive, 2 amyloid-negative). As expected, patients with MCI had significantly worse scores on the Montreal Cognitive Assessment (MoCA) (*P* = 0.02) and Word List Recall memory test (*P* = 0.04), as well as lower bilateral MTL volume (*P* < 0.05) compared to CN participants (Table 1).

Elevated MTL ^{11}C-Acetate in MCI

Despite these distinctions, there was no significant global difference in ^{11}C-acetate SUVR between MCI and CN groups (*P* = 0.50). However, lack of global ^{11}C-acetate elevation does not preclude a localized astrocyte response to amyloid. *Ex vivo* glial activation has been noted in the hippocampus, a critical memory node within the medial temporal lobe (MTL) [6]. Indeed, post-mortem biomarker expression analysis revealed elevations of astrocyte and acetate metabolism markers in the hippocampi of patients with AD relative to CN participants (Figure S3). See Supplementary Methods for additional information.

Thus, we hypothesized that MTL ^{11}C-acetate retention is elevated in MCI participants with amyloid pathology. We found that participants with MCI had significantly higher mean ^{11}C-acetate SUVR in the MTL (0.99±0.06) compared to CN participants (0.91±0.02; Cohen *d* = 1.76; *P* = 0.03) (Table 1, Figure 1). The magnitude of this observation is consistent

with effect sizes of other glial activation radiotracers; indeed, Cohen *d* effect sizes of regional ^{11}C-PBR28 activity range from 0.8-1.7 [48]. Additionally, limbic structures, such as cingulate and fusiform gyri, trended towards modest ^{11}C-acetate elevation in MCI (Figure 2, Table S1). These findings were replicated with KiR data (Table S2). The time stability curve (Figure S4) further depicts relatively stable V_T from 40-60 minutes consistent with non-accumulation of labelled metabolites, such that activity uptake and washout is likely due to the parent radiotracer.

Association of ^{11}C-Acetate and Amyloid PET

Our cohort was also tested for amyloid plaque levels by *in vivo* PET (Figure S5). Since overall neocortical amyloid deposition is associated with localized MTL neurodegeneration and neuroinflammation [49], we further examined the relationships between ^{11}C-acetate in the MTL and global amyloid burden in the supratentorial gray matter. MTL ^{11}C-acetate was positively correlated with global amyloid burden in the MCI group ($R = 0.83$; $P = 0.04$) but not in the normal cognition group (Figure 3A,B). These results were consistent with KiR data (Figure 3C,D). The differences in correlations of the CN and MCI groups by Fisher R-to-Z transformation were statistically significant (P values < 0.05), thereby supporting a potential association between local astrocyte activity and amyloid burden in MCI.

Activated astrocytes co-localize with amyloid plaques in several neuropathological studies [3,4,49], so we hypothesized that we would find greater ^{11}C-acetate retention in regions with greater amyloid burden. Since amyloid deposition varies between and within subjects, we studied regional association of astrocyte activation and amyloid across participants and regions with ^{11}C-acetate and ^{18}F-florbetaben amyloid PET, respectively, as a mixed linear effects model (Figure S6A,B). Intriguingly, for cognitively normal (CN) participants, regional ^{11}C-acetate retention revealed a significant negative association with regional amyloid deposition ($R = -0.36$; $P < 0.001$). For MCI, regional ^{11}C-acetate positively associated with regional amyloid ($R = 0.33$; $P < 0.001$). Between CN and MCI cohorts, significant group differences were noted for comparisons of both correlations and slopes (P values < 0.01). Furthermore, these amyloid correlation findings were replicated with ^{11}C-acetate kinetic data (Figure S6C-F). With the ^{11}C-acetate flux measures, differences between both correlations and slopes for CN and MCI were also significant (P values < 0.01).

Association of MTL ^{11}C-Acetate and Cognition

Next, we determined how MTL ^{11}C-acetate varied with cognition, including tests sensitive to episodic memory (Figure 4). Across all participants, elevated MTL ^{11}C-acetate SUVR was significantly associated with worse cognitive performance on tests such as the MoCA ($R = -0.84$; $P = 0.001$), Word List Recall memory ($R = -0.67$; $P = 0.03$), BNT ($R = -0.61$; $P = 0.04$) and Trails B Test ($R = 0.66$; $P = 0.04$).

After excluding CN participants from the regression analysis, associations between ^{11}C-acetate and cognition in participants with MCI remained significant for the MoCA ($P = 0.02$) and trended towards significance with Word List Recall ($P = 0.05$; Figure S7). The KiR flux replicated significant associations between ^{11}C-acetate and cognition for the

MoCA, BNT and Trails B Test (P values < 0.05), with a trend for Word List Recall (P = 0.08) (Figure S8).

DISCUSSION

This exploratory pilot study assessed ^{11}C-acetate PET as a biomarker in MCI with amyloid pathology. Astrocyte activation is seen on post-mortem assessments in early AD [1-4], however *in vivo* imaging of astrocyte metabolism biomarkers has not been surveyed extensively. Acetate uptake characterizes proliferating astrocytes [8,9,12-16] and may measure astrocyte activation in MCI. Overall, our findings depict regional correlation between amyloid and ^{11}C-acetate retention. Activation in the MTL also correlates with a global pattern of amyloid.

The MTL has been shown to be a hotspot of neuroinflammation in cognitive impairment and neurodegeneration [3-6,23,49,50]; this is concordant with our post-mortem expression analysis and *in vivo* ^{11}C-acetate imaging study. In addition to the significant group difference in the MTL, there is a general though modest elevation of ^{11}C-acetate retention across additional limbic brain regions, though this observation is limited by the exploratory nature of the pilot study. Notably, similar effect sizes are seen with other radiotracers of glial activity such as ^{11}C-PBR28 [7,29,30,48]. Limbic regions were shown in one study to have higher amyloid load and microglial inflammation in AD [7]; here, they displayed modest trends towards ^{11}C-acetate elevation in MCI. Consistent with other inflammation radiotracers [7,29,30], this trend may represent a relatively wider increase of astrocyte activity associated with diffuse cerebral amyloid pathology. However, the MTL might have the most discernible effect size for participants with MCI and early AD. Our pilot study was only sufficiently powered to detect an average ^{11}C-acetate SUVR difference of about 0.1. Based off prior ^{11}C-acetate neuroimaging studies, such a difference is consistent with disease-associated astrocyte activation [14,16].

The associations of ^{11}C-acetate, amyloid and clinical status are intricate. Significant elevation of MTL ^{11}C-acetate was found in participants with MCI; this effect is opposite of the well-known AD-related neuronal metabolic reductions measured with ^{18}F-fluorodeoxyglucose PET but compatible with prior literature on acetate as a biomarker of astrocyte activation [12-16]. Previous gene-expression studies have isolated distinct subtypes of reactive astrocytes, including pro-inflammatory, neurotoxic astrocytes enriched in AD and homeostatic astrocytes found in cognitively normal subjects [5,6]. While ^{11}C-acetate imaging may not be able to distinguish between distinct types of astrocyte activation, our observed associations of ^{11}C-acetate and amyloid retention are consistent with amyloid-induced, astrocyte-mediated inflammation [3-5]. Indeed, greater regional and global amyloid uptake were associated with higher regional ^{11}C-acetate in MCI, a correlation not mirrored in amyloid-positive, cognitively normal adults. Though additional studies are required, this directional difference raises the possibility that ^{11}C-acetate elevation is an astrocyte marker for the evolution of a proliferative inflammatory response and perhaps an amyloid-related neurodegenerative process in early AD that is not found in amyloid-positive, cognitively normal subjects. To this point, elevated MTL ^{11}C-acetate correlated with worse cognition, suggesting that ^{11}C-acetate is a marker of disease severity. Together, these *in vivo* imaging

and post-mortem expression findings indicate ^{11}C-acetate is a potential neuroinflammation marker of early astrocyte changes in early AD.

Our study has limitations. First, this exploratory pilot study had small sample size, limiting the power to detect changes in ^{11}C-acetate and perhaps increasing potential for sampling-related bias. Power in MCI vs. CN group comparisons was likely further reduced by the inclusion of amyloid-positive and amyloid-negative participants in the CN group. Nevertheless, this heterogeneous CN group more faithfully represents the variability of amyloid levels in cognitively unimpaired older adults and allows the evaluation of astrocyte activity in response to amyloid plaques at a dynamic range of subclinical amyloid burden. Next, the lack of detection of regional differences between MCI and CN groups outside the MTL may be due to sample size. Since this between-group effect size was modest, it is not clear that ^{11}C-acetate PET would be useful in all individual cases, at least in the absence of a separate amyloid PET study. Tau status was not known, and variability in pathological tau aggregates could potentially affect localization and extent of astrocyte activation [3,49,50]. Though it is possible that additional non-neuronal cells may contribute to ^{11}C-acetate uptake, much of the literature has focused on acetate uptake as an astrocyte marker [8,9,13]. Moreover, acetate metabolism is associated with reduced microglial activation [51], compared to greater astrocyte activity [8,9].

Additionally, PET signal was assessed using SUVR, kinetic flux and flux compared to cerebellum, which may correct for variability in tracer delivery, washout and background due to ^{11}C-acetate metabolism to $^{11}C-CO_2$ [14,16]. Time-activity curves stabilized after 20 minutes (Figure S2 and S4) and we measured SUVR from 40-60 minutes, consistent with previous studies [9,14]. At this later time point after ^{11}C-acetate injection, most of the signal was likely attributed to ^{11}C radionuclide from the parent tracer incorporated into macromolecules and thus represents a measure of astrocyte anabolic function and proliferative activity rather than a marker of just astrocyte energy catabolism or accumulation of radiometabolite alone. This is consistent with prior *in vivo* PET studies of homeostatic and proliferative astrocytes in healthy brains and patients with glioma [52,53]. Utilizing radiotracers that produce $^{11}C-CO_2$ metabolites (such as ^{11}C-thymidine), these studies have demonstrated a relatively ubiquitous $^{11}C-CO_2$ uptake with minimal tissue trapping similar to the results seen here. We had predicted that the lack of arterial input may impact the quality of the data used in the kinetic flux analysis, which was confirmed by our observation of inter-subject variability in Ki measurements (Figure S6). Thus, we utilized a flux measure [36-40] compared to cerebellar GM [29-31] to address such biases. In addition to quality of the data used, another limitation may pertain to the analytical approach. These findings suggest that the assumption of the Patlak method, that the radiotracer irreversibly binds to the specific target ($k_4 = 0$) from injection until the end of the imaging session, may not be entirely appropriate here, and may be related to the reversible exchange and lack of tissue trapping of the metabolite $^{11}C-CO_2$. Hence, the flux ratio was utilized to reduce potential biases related to data and model limitations when comparing between participants and further work will compare the flux ratio to methods that do not require irreversible binding using ^{11}C-acetate PET data acquired with arterial blood sampling and metabolite analysis.

Future directions include the validation of these pilot study results with a larger cohort of study participants and longitudinal study design. Given the differences in dynamic ranges and spatial localization of ^{11}C-acetate and ^{18}F-florbetaben uptake, additional studies may acquire multiple scans to evaluate test-retest variability and changes over time to further illuminate the dynamic pathophysiological processes in early AD. Correlation of astrocyte activation through ^{11}C-acetate PET with additional molecular imaging markers (such as tau PET) and post-mortem neuropathological assessment can also strengthen these findings.

CONCLUSIONS

This exploratory pilot imaging study in patients with amnestic MCI due to Alzheimer pathology suggests that astrocyte activation is associated with amyloid burden and can be detected with ^{11}C-acetate PET. We observed relationships between regional amyloid deposition with ^{11}C-acetate retention across the brain as well as associations between global amyloid burden with ^{11}C-acetate in the medial temporal lobe. Further, medial temporal lobe ^{11}C-acetate was significantly higher in participants with MCI and correlated with cognition. This study was limited by small sample size and larger trials with follow-up analyses and additional testing modalities are warranted. Together, ^{11}C-acetate imaging may be a biomarker of early astrocyte activation in neurodegeneration.

Supplementary Material

Refer to Web version on PubMed Central for supplementary material.

REFERENCES

1. Alzheimer A Über eine eigenartige Erkrankung der Hirnrinde. Allg Z Psychiat. 1907;64:146–148.

2. Fischer O Miliare Nekrosen mit drusigen Wucherungen der Neurofibrillen, eien regelmässige Veränderung der Hirnrinde bei seniler Demenz. Monatsschr Psychiat Neurol. 1907;22:361–372.

3. De Strooper B, Karran E. The Cellular Phase of Alzheimer's Disease. Cell. 2006;164(4):603–615.

4. Serrano-Pozo A, Muzikansky A, Gomez-Isla T, et al. Differential relationships of reactive astrocytes and microglia to fibrillar amyloid deposits in Alzheimer disease. J Neuropathol Exp Neurol. 2013 72(6):462–471. [PubMed: 23656989]

5. Lin Y-T, Seo J, Gao F, et al. APOE4 Causes Widespread Molecular and Cellular Alterations Associated with Alzheimer's Disease Phenotypes in Human iPSC-Derived Brain Cell Types. Neuron. 2018;98:1141–1154. [PubMed: 29861287]

6. Liddelow SA, Guttenplan KA, Clarke LE, et al. Neurotoxic reactive astrocytes are induced by activated microglia. Nature. 2017;541(7638):481–487. [PubMed: 28099414]

7. Parbo P, Ismail R, Hansen KV, et al. Brain inflammation accompanies amyloid in the majority of mild cognitive impairment cases due to Alzheimer's disease. Brain. 2017;140(7):2002–2011. [PubMed: 28575151]

8. Muir D, Berl S, Clarke DD. Acetate and fluoroacetate as possible markers for glial metabolism in vivo. Brain Res. 1986;380(2):336–340. [PubMed: 3756485]

9. Wyss MT, Magistretti PJ, Buck A, et al. Labeled acetate as a marker of astrocytic metabolism. J Cereb Blood Flow Metab. 2011;31(8):1668–1674. [PubMed: 21654698]

10. TCW J, Liang SA, Qian L, et al. Cholesterol and matrisome pathways dysregulated in human APOE ε4 glia. bioRχiv, 2019.

11. Farmer BC, Kluemper J, Johnson LA, Apolipoprotein E4 Alters Astrocyte Fatty Acid Metabolism and Lipid Droplet Formation. Cells. 2019;8(2):182.

12. Jiang L, Gulanski BI, De Feyter HM, et al. Increased brain uptake and oxidation of acetate in heavy drinkers. J Clin Invest. 2013;123(4):1605–1614. [PubMed: 23478412]

13. Mashimo T, Pichumani K, Vemireddy V, et al. Acetate is a bioenergetic substrate for human glioblastoma and brain metastases. Cell. 2014;159(7):1603–1614. [PubMed: 25525878]

14. Takata K, Kato H, Shimosegawa E, et al. ^{11}C-acetate PET imaging in patients with multiple sclerosis. PLOS ONE. 2014;9(11):e111598. [PubMed: 25369426]

15. Volkow ND, Kim SW, Wang GJ, et al. Acute alcohol intoxication decreases glucose metabolism but increases acetate uptake in the human brain. Neuroimage. 2013;64:277–283. [PubMed: 22947541]

16. Yamamoto Y, Nishiyama Y, Kimura N. ^{11}C-acetate PET in the evaluation of brain glioma: comparison with ^{11}C-methionine and ^{18}F-FDG-PET. Mol Imaging Biol. 2008;10(5):281–287. [PubMed: 18543041]

17. Pike VW, Eakins MN, Allan RM, Selwyn AP, Preparation of [1-^{11}C]acetate-an agent for the study of myocardial metabolism by positron emission tomography. Int J Appl Radiat Isot. 1982;33(7):505–512. [PubMed: 6981606]

18. Tzourio-Mazoyer N, Landeau B, Papathanassiou D, et al. Automated anatomical labeling of activations in SPM using a macroscopic anatomical parcellation of the MNI MRI single-subject brain. NeuroImage. 2002;15(1):273–289. [PubMed: 11771995]

19. Aston JA, Cunningham VJ, Asselin MC, et al. Positron emission tomography partial volume correction: estimation and algorithms. J Cereb Blood Flow Metab. 2002;22(8):1019–1034. [PubMed: 12172388]

20. Ikonomovic MD, Buckley CJ, Heurling K, et al. Post-mortem histopathology underlying β-amyloid PET imaging following flutemetamol F18 injection. Acta Neuropathol Commun. 2–16;4:130.

21. Raji CA, Becker JT, Tsopelas ND, et al. Characterizing regional correlation, laterality and symmetry of amyloid deposition in mild cognitive impairment and Alzheimer's disease with Pittsburgh Compound B. J Neurosci Methods. 2008;172:277–282. [PubMed: 18582948]

22. Moossy J, Zubenko GS, Martinez AJ, et al. Bilateral symmetry of morphologic lesions in Alzheimer's disease. Arch Neurol. 1988;45(3):251–254. [PubMed: 3341948]

23. Johnson KA, Fox NC, Sperling RA and Klunk WE. Brain Imaging in Alzheimer Disease. Cold Spring Harb Perspect Med, 2012:a006213. [PubMed: 22474610]

24. Kolthammer JA, Su KH, Grover A, et al. Performance evaluation of the ingenuity TF PET/CT scanner with a focus on high count-rate conditions. Phys Med Biol. 2014;59(14):3843–3859. [PubMed: 24955921]

25. Grassi I, Nanni C, Allegri V, et al. The clinical use of PET with ^{11}C-acetate. Am J Nucl Med Mol Imaging. 2012;2(1):33–47. [PubMed: 23133801]

26. Catafau AM, Bullich S, Seibyl JP, et al. Cerebellar Amyloid-β Plaques: How Frequent Are They, and Do They Influence ^{18}F-Florbetaben SUV Ratios? J Nucl Med. 2016;57:1740–1745. [PubMed: 27363836]

27. Sabri O, Seibyl J, Rowe C, Barthel H. Beta-amyloid imaging with florbetaben. Clin Transl Imaging. 2015;3:13–26. [PubMed: 25741488]

28. Weigel J, Wisniewski HM, Dziewiatkotski J, et al. Cerebellar Atrophy in Alzheimer's Disease-Clinicopathological Correlations. Brain Res. 1999;6(818):41–50.

29. Rodriguez-Vieitez E, Saint-Aubert L, Carter SF, et al. Diverging longitudinal changes in astrocytosis and amyloid PET in autosomal dominant Alzheimer's disease. Brain. 2016;139:922–936. [PubMed: 26813969]

30. Scholl M, Carter SF, Westman E, et al. Early astrocytosis in autosomal dominant Alzheimer's disease measured in vivo by multi-tracer positron emission tomography. Sci Rep. 2015;5:16404. [PubMed: 26553227]

31. Carter SF, Scholl M, Almkvist O, et al. Evidence for astrocytosis in prodromal Alzheimer disease provided by ^{11}C-deuterium-L-deprenyl: a multitracer PET paradigm combining ^{11}C-Pittsburgh compound B and ^{18}F-FDG. J Nucl Med. 2012;53:37–46. [PubMed: 22213821]

32. O'Sullivan F, Muzi M, Mankoff DA, Eary JF, Spence AM and Krohn KA. Voxel-Level Mapping of Tracer Kinetics in PET Studies: a Statistical Approach Emphasizing Tissue Life Tables. Ann Appl Stat. 2014;8(2):1065–1094. [PubMed: 25392718]

33. Patlak CS, Blasberg RG and Fenstermacher JD. Graphical Evaluation of Blood-to-Brain Transfer Constants from Multiple-Time Uptake Data. J Cereb Blood Flow Metab. 1983;3:1–7. [PubMed: 6822610]

34. Patlak CS, Blasberg RG. Graphical Evaluation of Blood-to-Brain Transfer Constants from Multiple-Time Uptake Data. Generalizations. J Cereb Blood Flow Metab. 1985;5:584–590. [PubMed: 4055928]

35. Zanotti-Fregonara P, Chen K, Liow J-S, Fujita M and Innis RB. Image-derived input function for brain PET studies: many challenges and few opportunities. J Cereb Blood Flow Metab. 2011;31(10):1986–1998. [PubMed: 21811289]

36. Dhawan V, Ma Y, Pillai V, et al. Comparative Analysis of Striatal FDOPA Uptake in Parkinson's Disease: Ratio Method Versus Graphical Approach. J Nucl Med. 2002;43(10):1324–1330. [PubMed: 12368370]

37. Kawatsu S, Kato T, Nagano-Saito A, Hatano K, Ito K and Ishigaki T. New Insight Into the Analysis of 6-[^{18}F]fluoro-L-DOPA PET Dynamic Data in Brain Tissue Without an Irreversible Compartment: Comparative Study of the Patlak and Logan Analyses. Radiat Med. 2003;21(1):47–54. [PubMed: 12801143]

38. Alves IL, Meles SK, Willemsen ATM, et al. Dual time point method for the quantification of irreversible tracer kinetics: A reference tissue approach applied to [18F]-FDOPA brain PET. J Cereb Blood Flow Metab. 2017;37(9):3124–3134. [PubMed: 28156211]

39. Zhou Y, Ye W, Braši JR, Wong DF. Multi-graphical analysis of dynamic PET. Neuroimage. 2010;49(4):2947–2957. [PubMed: 19931403]

40. Wu YG, Zhou Y, Bao BL, et al. Using the rPatlak plot and dynamic FDG-PET to generate parametric images of relative local cerebral metabolic rate of glucose. Sci Bull. 2020;57:3811–3818.

41. Logan J, Fowler JS, Volkow ND, et al. Distribution Volume Ratios Without Blood Sampling from Graphical Analysis of PET Data. J Cereb Blood Flow Metab 1996;16(5):834–840. [PubMed: 8784228]

42. Morris JC, Heyman A, Mohs RC, et al. The Consortium to Establish a Registry for Alzheimer's Disease (CERAD). Part I. Clinical and neuropsychological assessment of Alzheimer's disease. Neurology. 1989;39:1159–1165. [PubMed: 2771064]

43. Nasreddine ZS, Phillips NA, Bédirian V, et al. The Montreal Cognitive Assessment, MoCA: A Brief Screening Tool For Mild Cognitive Impairment. J Am Geriatr Soc. 2005;53(4):695–699. [PubMed: 15817019]

44. Kaplan E, Goodglass H and Weintraub S. The Boston Naming Test. Lea & Febiger, Philadelphia, PA, 1983.

45. Reitan RM. Trail Making Test: Manual for administration and scoring. Reitan Neuropsychology Laboratory, Tucson, AZ,1992.

46. Schmidt M Rey Auditory Verbal Learning Test: RAVLT: a handbook. Western Psychological Services, Los Angeles, CA, 1996.

47. Pinhheiro J, Bates D, Debroy S, Sarkar D and R Core Team. nlme: Linear and Nonlinear Mixed Effects Models. 3rd. ed., 2016.

48. Bloomfield PS, Selvaraj S, Veronese M, et al. Microglial activity in people at ultra high risk of psychosis and in schizophrenia; an [11C]PBR28 PET brain imaging study. Am J Psychiatry. 2016;173(1):44–52. [PubMed: 26472628]

49. Kinney JW, Bemiller SM, Murtishaw AS, et al. Inflammation as a central mechanism in Alzheimer's disease. Alzheimers Dement. 2018;4:575–590.

50. Duong MT, Nasrallah IM, Wolk DA, Chang CCY and Chang T-Y. Cholesterol, Atherosclerosis, and APOE in Vascular Contributions to Cognitive Impairment and Dementia (VCID): Potential Mechanisms and Therapy. Front Aging Neurosci. 2021;13:647990. [PubMed: 33841127]

51. Soliman ML, Puig KL, Combs CK and Rosenberger TA. Acetate reduces microglia inflammatory signaling in vitro. J Neurochem. 2013;123(4):555–567.

52. Wells JM, Mankoff DA, Muzi M, O'Sullivan F, Eary JF, Spence AM, Krohn KA. Kinetic analysis of 2-[11C]thymidine PET imaging studies of malignant brain tumors: compartmental model investigation and mathematical analysis. Mol Imaging. 2002 Jul;1(3):151–9. [PubMed: 12920853]

53. Wells JM, Mankoff DA, Eary JF, Spence AM, Muzi M, O'Sullivan F, Vernon CB, Link JM, Krohn KA. Kinetic analysis of 2-[11C]thymidine PET imaging studies of malignant brain tumors: preliminary patient results. Mol Imaging. 2002 Jul;1(3):145–50. [PubMed: 12920852]
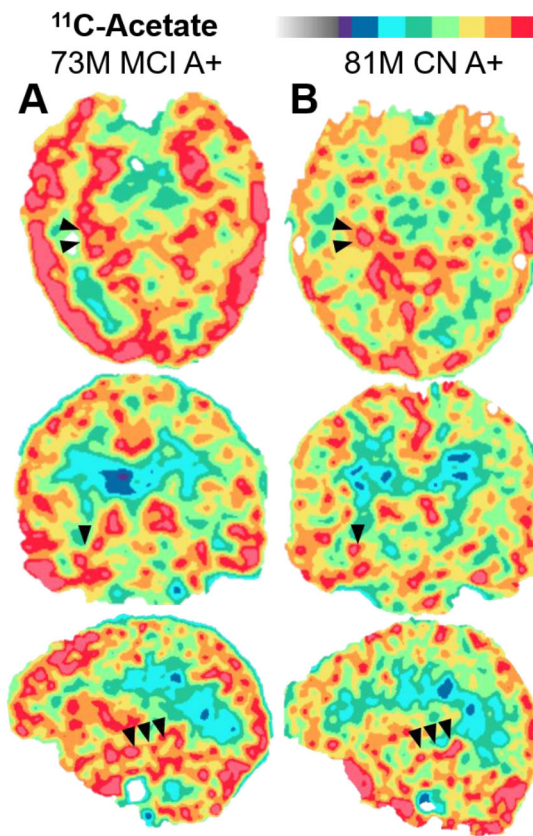
FIGURE 1.
Example ^{11}C-acetate SUVR maps in representative amyloid-positive (A+) participants with (**A**) mild cognitive impairment (MCI) or (**B**) normal cognition (CN). Arrowheads depict the hippocampus in the right medial temporal lobe.
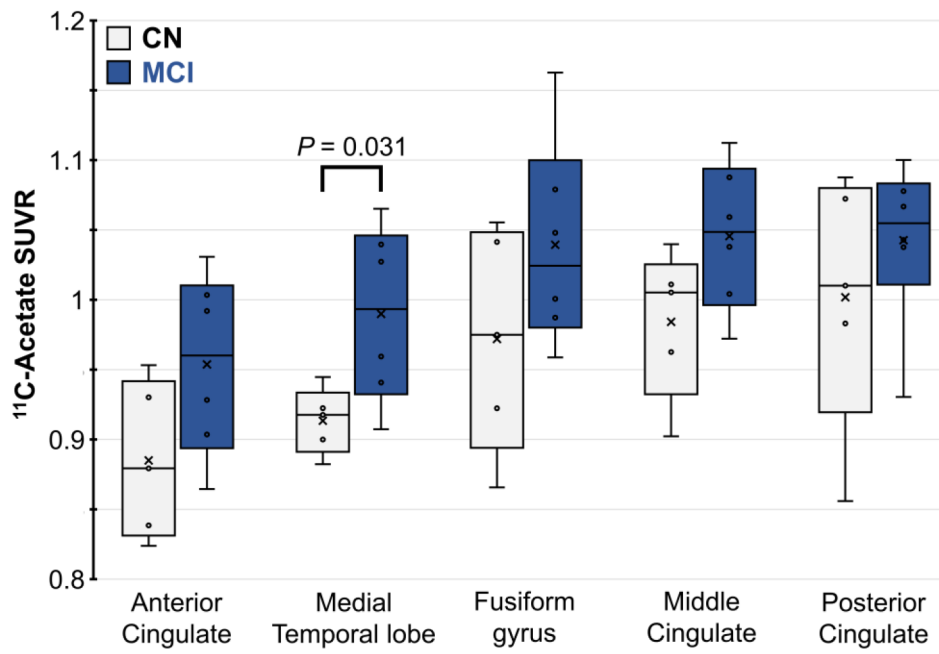
FIGURE 2.
[11]C-Acetate SUVR in limbic brain ROIs of participants with MCI (blue) and normal cognition (CN, gray). *P* values < 0.05 are shown.
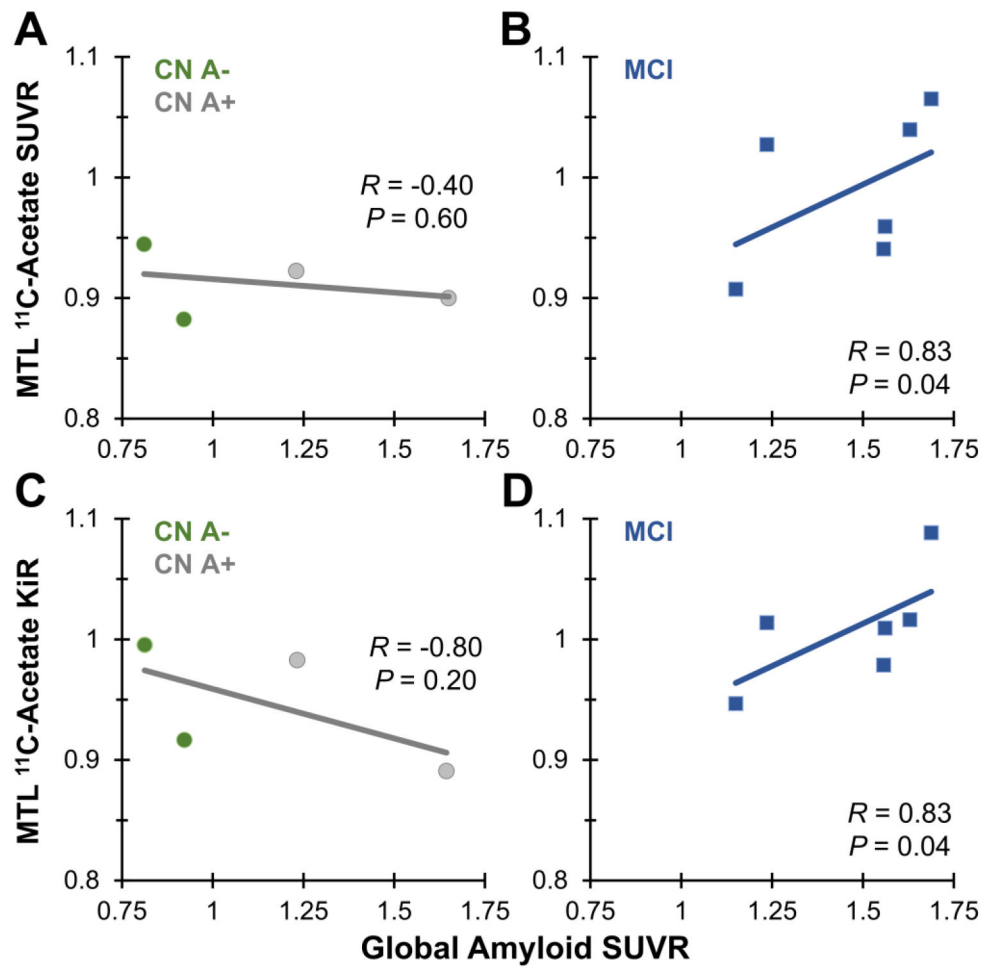
FIGURE 3.

Comparison of MTL ^{11}C-acetate SUVR vs. global amyloid SUVR in (**A**) 4 CN and (**B**) 6 MCI participants. Comparison of MTL ^{11}C-acetate Patlak flux ratio (KiR) vs. global amyloid SUVR in (**C**) 4 CN and (**D**) 6 MCI participants. Linear regressions, Spearman correlations and *P* values are shown.
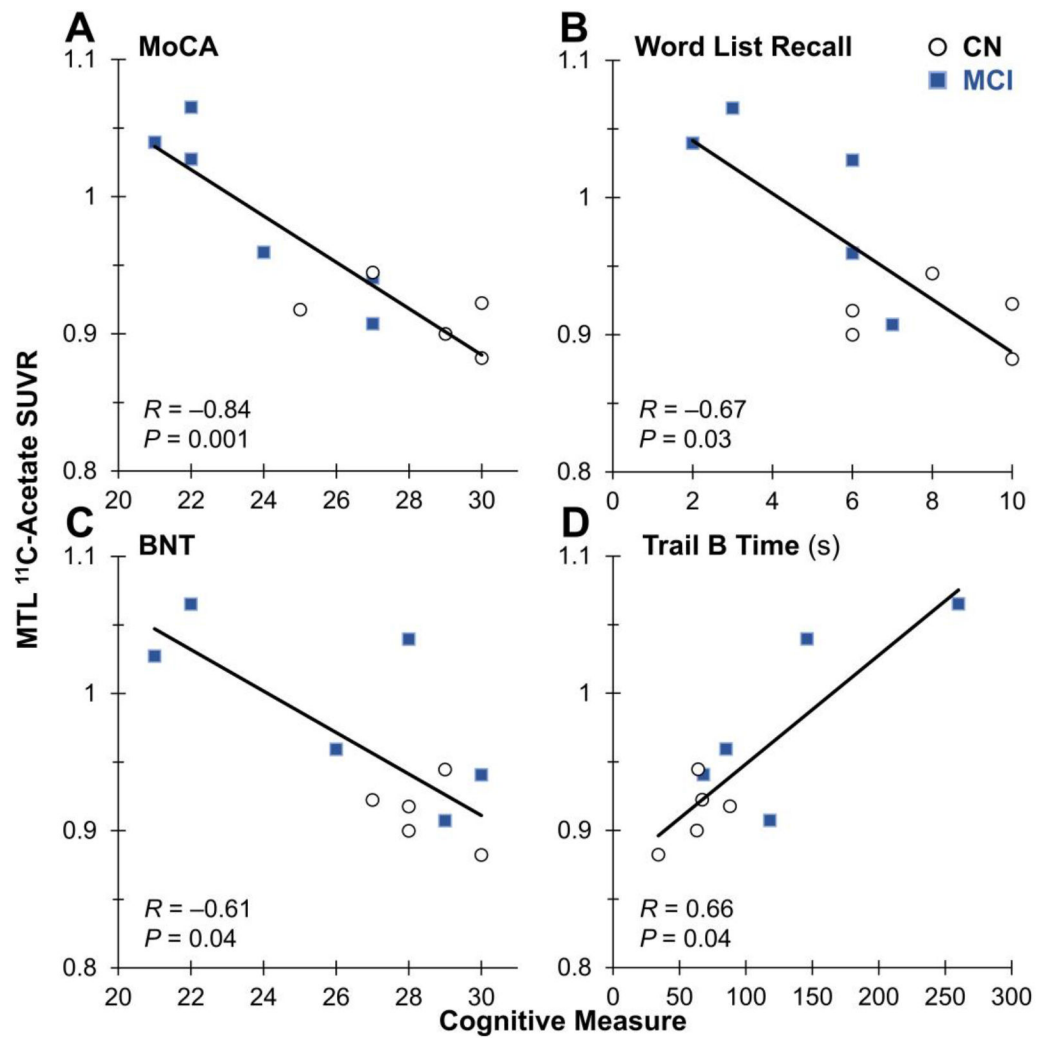
FIGURE 4.
Comparison across all participants of MTL ^{11}C-acetate SUVR vs. cognitive tests of (**A**) Montreal Cognitive Assessment (MoCA), (**B**) Word List Recall (a test of hippocampal memory), (**C**) Boston Naming Test (BNT) and (**D**) Trails B time (in seconds). Linear regressions, Spearman correlations and *P* values are shown.

TABLE 1.

Study participant characteristics. Abbreviations: standard deviation (SD), Montreal Cognitive Assessment (MoCA), Boston Naming Test (BNT), medial temporal lobe (MTL). *P* values are from 2-sample independent *t*-tests.

Study Characteristic	Cognitively Normal	MCI	*P* value
Total participants	5	6	
Female (%)	2 (40%)	4 (67%)	
Age, mean (SD) [range], years	74 (10) [61-85]	72 (6) [65-84]	0.75
Amyloid PET positive (%)	3 (60%)	6 (100%)	
MoCA, mean (SD) [range]	29 (2) [25-30]	24 (2) [21-27]	0.02
Word List Recall, mean (SD) [range]	8 (2) [6-10]	5 (2) [2-7]	0.04
BNT, mean (SD) [range]	28 (1) [27-30]	26 (4) [21-30]	0.20
Trails Time, mean (SD) [range], seconds	63 (19) [34-88]	135 (76) [68-260]	0.07
MTL Volume, mean (SD), cm^3	16.1 (1.9)	13.5 (1.9)	<0.05